



1 **A New Method for Calculating Number Concentrations of Cloud**
2 **Condensation Nuclei Based on Measurements of A Three-wavelength**
3 **Humidified Nephelometer System**

4 Jiangchuan Tao¹, Chunsheng Zhao¹, Ye Kuang¹, Gang Zhao¹, Chuanyang Shen¹, Yingli Yu¹, Yuxuan
5 Bian², Wanyun Xu²

6 [1]{Department of Atmospheric and Oceanic Sciences, School of Physics, Peking University, Beijing,
7 China}

8 [2]{State Key Laboratory of Severe Weather, Chinese Academy of Meteorological Sciences}

9 *Correspondence to: C. S. Zhao (zcs@pku.edu.cn)

10 Abstract

11 The number concentration of cloud condensation nuclei (CCN) plays a fundamental role in
12 cloud physics. Instrumentations of direct measurements of CCN number concentration (N_{CCN}) based
13 on chamber technology are complex and costly, thus a simple way for measuring N_{CCN} is needed. In
14 this study, a new method for N_{CCN} calculation based on measurements of a three-wavelength
15 humidified nephelometer system is proposed. A three-wavelength humidified nephelometer system
16 can measure aerosol light scattering coefficient (σ_{sp}) at three wavelengths and the light scattering
17 enhancement factor (fRH). The Angstrom exponent (\AA) inferred from σ_{sp} at three wavelengths
18 provides information on mean predominate aerosol size and hygroscopicity parameter (κ) can be
19 calculated from the combination of fRH and \AA . Given this, a look-up table that involves σ_{sp} , κ and
20 \AA is established to predict N_{CCN} . This method is validated with direct measurements of N_{CCN} using a
21 CCN counter on the North China Plain. Results show that relative deviations between calculated
22 N_{CCN} and measured N_{CCN} are within 30% and confirm the robustness of this method. This method
23 enables simpler N_{CCN} measurements because the humidified nephelometer system is easily operated
24 and stable. Compared with the method of CCN counter, another advantage of this newly proposed
25 method is that it can obtain N_{CCN} at lower supersaturations in the ambient atmosphere.

26



27 1. Introduction

28 Cloud condensation nuclei (CCN) is the aerosol particle forming cloud droplet by hygroscopic
29 growth. CCN number concentration (N_{CCN}) plays a fundamental role in cloud micro physics and
30 aerosol indirect radiative effect. In general, the direct measurement of N_{CCN} is achieved in a cloud
31 chamber under super-saturated conditions (Hudson, 1989;Nenes et al., 2001;Rose et al., 2008). Due
32 to the requirement of high accuracies of working conditions like temperatures, vapors and flow rates
33 in cloud chambers, the direct measurement of N_{CCN} is complex and costly (Rose et al., 2008;Latham
34 and Nenes, 2011). Thus, developments of simplified measurements of N_{CCN} are required. In recent
35 years, attention has been focused on measurements of aerosol optical properties (Jefferson,
36 2010;Ervens et al., 2007;Gasso and Hegg, 2003), which are simple and well-developed (Covert et al.,
37 1972;Titos et al., 2016). For aerosol population free of sea salt or dust, the accumulation mode
38 aerosol not only dominates aerosol scattering ability but also contribute most to N_{CCN} . Thus, the
39 calculation of N_{CCN} based on measurements of aerosol optical properties is feasible, and can facilitate
40 N_{CCN} measurement.

41 There are two kinds of methods to calculating N_{CCN} based on measurements of aerosol optical
42 properties. For the first kind, N_{CCN} as well as the hygroscopicity parameter (κ) can be calculated
43 based on measurements of a humidified nephelometer system in combination with aerosol particle
44 number size distribution (PNSD) (Ervens et al., 2007;Chen et al., 2014). Thus additional
45 measurements of PNSD are needed. For the second kind, N_{CCN} is calculated based on statistical
46 relationships between N_{CCN} and aerosol optical properties, such as scattering coefficient (σ_{sp}),
47 Angstrom Exponent (\AA) and single scattering albedo (SSA) (Jefferson, 2010;Shinozuka et al., 2015).
48 Compared with the first kind, instruments used in the second kind of methods are cheaper and easier
49 in operation. Applications similar to the second kind are widely used in remote sensing. Earlier
50 studies found that the aerosol volume or aerosol PNSD retrieved from remote sensing measurements
51 can be used to calculate N_{CCN} (Gasso and Hegg, 2003;Kapustin et al., 2006). Recently, aerosol
52 optical depth (AOD) or aerosol vertical profile is used to predict N_{CCN} directly(Ghan and Collins,
53 2004;Ghan et al., 2006;Andreae, 2009;Liu and Li, 2014).

54 In the statistical relationship between N_{CCN} and aerosol optical properties, σ_{sp} or AOD is mainly



55 the proxy of aerosol absolute concentration, while \dot{A} or SSA can be used to reveal the variations of
56 aerosol CCN activity. Based on Kohler theory (Köhler, 1936; Petters and Kreidenweis, 2007), aerosol
57 CCN activity is determined by aerosol size and aerosol chemical composition which is defined as
58 aerosol hygroscopicity. Information about aerosol size and aerosol hygroscopicity are critical to N_{CCN}
59 prediction and their absence can lead to a deviation with factor of four (Andreae, 2009). Compared
60 with aerosol hygroscopicity, aerosol size is more important in determining CCN activity (Dusek et al.,
61 2006). The value of \dot{A} can provide information on mean predominate aerosol size (Brock et al.,
62 2016; Kuang et al., 2017). As a result, N_{CCN} calculation from \dot{A} and extinction coefficient is found to
63 be accurate to some extent (Shinozuka et al., 2015). As proxies for aerosol hygroscopicity, SSA or
64 aerosol light scattering enhancement factor (fRH) is commonly used while not so effective. SSA is
65 determined by the ratio between the light absorbing carbonaceous and less-absorbing components.
66 Black carbon contributes most to the light absorbing carbonaceous and is the most important
67 hydrophobic compositions as well. Less-absorbing components consist of inorganic salts and acids,
68 as well as most organic compounds, which are generally hygroscopic compositions. SSA correlates
69 positively with aerosol hygroscopicity (Rose et al., 2010) but deviates significantly due to the
70 diversity of hygroscopicity of less-absorbing components. Thus deviations of N_{CCN} calculation based
71 on SSA is of large errors (Jefferson, 2010). Compared with SSA, previous studies found fRH to be
72 less effective in estimating N_{CCN} , even though fRH directly connected with aerosol hygroscopicity
73 (Liu and Li, 2014). This may result from the significant dependence of fRH on aerosol size (Chen et
74 al., 2014; Kreidenweis and Asa-Awuku, 2014; Kuang et al., 2017). As mentioned before, PNSD is
75 used for better calculation of κ and N_{CCN} from fRH in previous studies (Ervens et al., 2007; Chen et
76 al., 2014). A new method to estimate κ from fRH and \dot{A} was proposed recently (Kuang et al.,
77 2017; Brock et al., 2016). Based on this method, fRH can be used to calculate N_{CCN} without
78 measurements of PNSD and can be expected to improve the N_{CCN} prediction just based on
79 measurements of aerosol optical properties.

80 In this study, the relationship between N_{CCN} and aerosol optical properties measured by a
81 humidified nephelometer system is studied and a new method for N_{CCN} prediction is proposed. This
82 new method is validated based on data observed in Gucheng campaign on the North China Plain and
83 can be expected to improve measurements of N_{CCN} due to advantages of applying nephelometers.



84

85 2. Methodology

86 2.1. Data

87 Data in this study are mainly measured at Gucheng (39.15N, 115.74E) during autumn in 2016
88 on the North China Plain (NCP). Gucheng is 100km southwest from Beijing and 40km northeast
89 from Baoding under background pollution condition in the NCP. The observation site was
90 surrounded by farmland and about 3km away from the Gucheng town. This campaign started on 20
91 October and lasted for nearly one month.

92 Instruments used in Gucheng campaign were located in a measurement container under
93 temperature maintained at 25 °C. Ambient aerosol was sampled and dried to relative humidity (RH)
94 lower than 30% by a inlet system consist of a PM10 inlet, a inline Nafion dryers and a RH and
95 temperature sensor (Vaisala HMP110). Then the sample aerosol was separated by a splitter and
96 directed into various instruments. During this campaign, aerosol scattering coefficient (σ_{sp}), aerosol
97 optical hygroscopic growth factor (fRH), particle size-resolved activation ratio (AR) and particle
98 number size distribution (PNSD) were obtained.

99 fRH as well as σ_{sp} at three wavelengths were measured by a humidified nephelometer system
100 consisting of two nephelometers (Aurora 3000, Ecotech Inc.) and a humidifier. σ_{sp} can be described
101 by a formula of Å: $\sigma_{sp}(\lambda)=\beta\cdot\lambda^{-\text{Å}}$, where β is the aerosol number concentration and λ is the
102 wavelength. Thus Å can be calculated directly from σ_{sp} measured by a nephelometer. The
103 humidifier with a Gore-Tex tube humidified the sample air up to 90% RH. A whole cycle of
104 humidification lasted about 45minutes from 50% RH to 90% RH. Dried σ_{sp} was obtained directly
105 from dried sample aerosol measured by one nephelometer and humidified σ_{sp} was obtained from
106 humidified aerosol measured by another nephelometer. fRH is the ratio of the humidified σ_{sp} to the
107 dried σ_{sp} at each RH. Detailed description of the humidified nephelometer system was illustrated in
108 Kuang et al (2017).

109 The particle size-resolved AR, defined as the ratio of N_{CCN} to total particles, was measured by a



110 system mainly consisting of a differential mobility analyzer (DMA) and a continuous-flow CCN
111 counter (model CCN200, Droplet Measurement Technologies, USA; Roberts and Nenes
112 (2005); Lance et al., (2006)). The system selected mono-disperse particles with the DMA coupled
113 with a electrostatic classifier (model 3080; TSI, Inc., Shoreview, MN USA) and measured AR of the
114 mono-disperse particles by a condensation particle counter (CPC model 3776; TSI, Inc.) and CCN
115 counter. Ranges of particle size and supersaturation were 10-300nm and 0.07%-0.80%, respectively.
116 Measurements at five supersaturations were conducted sequentially and each cycle lasted for 1 hour.
117 Before and after the campaign, supersaturations set in this system were calibrated using ammonium
118 sulfate (Rose et al., 2008). More information about the system are given in Deng et al. (2011) and
119 Ma et al. (2016).

120 PNSD with particle diameter from 9nm to 10um was measured by a mobility particle size
121 spectrometer (SMPS, TSI Inc., Model 3996) and an Aerodynamic Particle Sizer (APS, TSI Inc.,
122 Model 3321). SMPS consisted of a DMA, a electrostatic classifier and a CPC (model 3776; TSI, Inc.,
123 Shoreview, MN USA) and measured PNSD with diameter lower than 700nm.

124 In addition, PNSD and σ_{sp} from 2011 to 2014 at four campaigns (Wuqing in 2011, Xianghe in
125 2012 and 2013, and Wangdu in 2014) in NCP were used in this study. PNSD in these campaigns was
126 measured by a Twin Differential Mobility Particle Sizer (TDMPS, Leibniz-Institute for Tropospheric
127 Research (IfT), Germany) and an Aerodynamic Particle Sizer (APS, TSI Inc., Model 3321). A TSI
128 3563 nephelometer was used to obtain σ_{sp} at three wavelengths. Details about the four campaign
129 can be found in Ma et al. (2011), Ma et al. (2016), Kuang et al. (2016) and Kuang et al. (2017).

130

131 2.2. Theories

132 Hygroscopic growth of particles at certain relative humidity can be described by κ -Köhler
133 theory (Petters and Kreidenweis, 2007):

$$134 \frac{RH}{100} = \frac{g(RH)^3 - 1}{g(RH)^3 - (1 - \kappa)} \cdot \exp\left(\frac{4\sigma_{s/a} \cdot M_w}{R \cdot T \cdot D_a \cdot g \cdot \rho_w}\right) \quad (1)$$

135 where $g(RH)$ is geometric diameter growth factor, κ is the hygroscopicity parameter, S is the
136 saturation ratio; ρ_w is the density of water; M_w is the molecular weight of water; $\sigma_{s/a}$ is the surface
137 tension of the solution–air interface, which is assumed to be equal to the surface tension of the pure



138 water–air interface; R is the universal gas constant; and T is the temperature.

139 Accounting for the impact of \mathring{A} , κ_f can be derived directly from fRH (Brock et al., 2016; Kuang
140 et al., 2017). A single-parameter parameterization scheme proposed by Brock et al. (2016) connects
141 fRH and κ by the approximately proportional relationship between total aerosol volume and σ_{sp} :

$$142 \quad f(RH) = 1 + \kappa_{sca} * RH / (100 - RH) \quad (2)$$

143 where κ_{sca} is a parameter for fitting fRH curves and can determine κ_f with \mathring{A} . This method was
144 confirmed by good agreement with κ_f calculated from fRH and $g(RH)$ (Brock et al., 2016; Kuang
145 et al., 2017).

146 N_{CCN} can be calculated from size-resolved AR at a certain supersaturation (SS) and PNSD
147 (referred to as $n(\log D_p)$) as follows:

$$148 \quad N_{CCN} = \int_{\log D_p} AR(\log D_p, SS) \cdot n(\log D_p) d \log D_p \quad (3)$$

149 In general, size-resolved AR curves are complicated and always replaced by a critical diameter to
150 simplify calculation (Deng et al., 2013). The critical diameter is defined as:

$$151 \quad N_{CCN} = \int_{\log D_c}^{\log D_{p,max}} n(\log D_p) d \log D_p \quad (4)$$

152 where $D_{p,max}$ is the maximum diameter of the measured particle number size distribution. In other
153 words, the integral of PNSD larger than D_c equals to the measured N_{CCN} . And a critical κ (κ_c) can be
154 calculated by equation (1) and indicated CCN activity and hygroscopicity of particles.

155

156 3. Results

157 3.1. Calculation of N_{CCN} based on measurements of a Humidified Nephelometer system

158 Free of sea salt aerosol and dust aerosol, accumulation mode aerosol dominates both the optical
159 scattering ability at short wavelength and the CCN activity at low supersaturation, and thus a
160 reasonable relationship between σ_{sp} and N_{CCN} can be achieved. Figure 1 shows the size distribution
161 of cumulative contributions of σ_{sp} at 450nm and N_{CCN} at 0.07% with various \mathring{A} and κ_c , and



162 corresponding normalized PNSDs based on data measured at the four campaigns on the North China
163 Plain. During the four campaigns, no sea salt aerosol or dust aerosol was observed (Ma et al.,
164 2011; Ma et al., 2016; Kuang et al., 2016; Kuang et al., 2017). For continental aerosol without sea salt
165 or dust, \bar{A} varies from 0.5 to 1.8 and κ_c varies from 0.1 to 0.5. And as mentioned before, \bar{A} can be
166 used as a proxy of the overall size distribution of aerosol populations, with smaller \bar{A} indicating
167 more larger particles. In figure 1, comparisons for \bar{A} are made between 0.5 and 1.7 and for κ_c are
168 made between 0.1 and 0.5. As larger particles contribute more to light scattering and activation,
169 cumulative contributions of both σ_{sp} and N_{CCN} increase significantly at the diameter range of
170 accumulation mode particles. Because more hygroscopic particles are able to activate at smaller
171 diameters, the cumulative contribution of N_{CCN} with higher κ_c increase at smaller diameters. In
172 general, major contributions of both σ_{sp} and N_{CCN} are made by particles from 200nm to 500nm for
173 various \bar{A} and κ_c . This implies the feasibility of inferring N_{CCN} from aerosol optical properties.

174 Because smaller particles can activate at higher supersaturations while scatter less light at longer
175 wavelengths, it's obvious that significant differences will exist between cumulative contributions of
176 σ_{sp} and N_{CCN} . This means σ_{sp} and N_{CCN} are dominated by different particles and poor correlation
177 between σ_{sp} and N_{CCN} can be expected. Thus the method of inferring N_{CCN} from aerosol optical
178 properties is applicable for shorter wavelength and lower supersaturations.

179 Furthermore, PNSD with higher \bar{A} indicates as more Aitken mode particles and fewer
180 accumulation mode particles. Thus large particles contribute less for both σ_{sp} and N_{CCN} when \bar{A} are
181 higher, characterizing an increase of cumulative contribution curves at smaller diameters. In detail,
182 differences between cumulative contribution curves with \bar{A} of 0.5 and 1.7 are about 150nm and
183 100nm for σ_{sp} and N_{CCN} , respectively. Changes of cumulative contributions of N_{CCN} and σ_{sp} with
184 various \bar{A} reveal that the shape of PNSD can influence the correlation between N_{CCN} and σ_{sp} . This
185 is confirmed by previous studies in which the \bar{A} is found to play an important role in calculating
186 N_{CCN} from σ_{sp} (Shinozuka et al., 2015; Liu and Li, 2014).

187 The relationship between σ_{sp} and N_{CCN} dependent on \bar{A} and κ_c is evaluated by calculating



188 σ_{sp} and N_{CCN} with different PNSDs classified by \dot{A} and different κ_c . In detail, ratios of N_{CCN} to σ_{sp} ,
189 referred to as AR_{sp} , are calculated to eliminate the effect of variations of particle concentrations
190 consistent at all diameters. Results at the supersaturation of 0.07% are shown in figure 2 and AR_{sp}
191 range from 0 to 10. In general, AR_{sp} are higher for more hygroscopic particles or smaller particles. As
192 particles become more hygroscopic, more CCN can be expected when σ_{sp} is fixed. As aerosol
193 populations consist of more smaller CCN-active particles, the increase of σ_{sp} is weaker than that of
194 N_{CCN} .

195 In detail, the sensitivity of AR_{sp} to \dot{A} also changes with \dot{A} and κ_c . When \dot{A} are higher than 1.4
196 and κ_c is lower than 0.2, AR_{sp} is insensitive to \dot{A} . While when \dot{A} are lower than 1 and κ_c are
197 higher than about 0.3, AR_{sp} is more sensitive to \dot{A} than κ_c . Higher sensitivity of AR_{sp} to \dot{A} are
198 found with higher κ_c and lower \dot{A} , which reveals that particles having more small particles and less
199 large particles than existing particles can contribute more to N_{CCN} . This is the consequence of the
200 sensitivity of AR_{sp} to \dot{A} resulting from the variation of small CCN-active particles, as mentioned
201 before.

202 Based on the lookup-table illustrated in Figure 2, N_{CCN} at the supersaturation of 0.07% can be
203 calculated simply from \dot{A} , κ_f and σ_{sp} which can be obtained from measurements of a humidified
204 nephelometer system. The description of this simple method is shown in figure 3. A new look-up
205 table needs to be made for N_{CCN} estimation at other supersaturations, which should better be less than
206 0.07% as mentioned in the discussion of figure 1.

207 One critical issue about the method is the conversion of the κ_f obtained from the humidified
208 nephelometer system to the κ_c under super-saturated conditions. There are mainly two factors
209 making this conversion necessary. First, closure studies of aerosol hygroscopicity found significant
210 deviations between hygroscopicity at sub-saturated conditions and super-saturated conditions. Their
211 difference can be expected to be about 0.1 for accumulation mode aerosol (Wu et al., 2013; Whitehead
212 et al., 2014; Ma et al., 2016). Second, the κ_f indicates the hygroscopicity of total particles and can be
213 quite different from aerosol hygroscopicity at a specific diameter due to variations of size
214 distributions of particle hygroscopicity. Kuang et al. (2017) found a difference around 0.1 between



215 κ_f and κ inferred from g(RH) measurements for accumulation mode particles whose κ_f is no larger
216 than 0.2. In this study, a simple conversion that κ_c is 0.2 higher than κ_f is used to calculate N_{CCN} ,
217 while for κ_f larger than 0.2, a smaller difference of 0.1 between κ_c and κ_f should be used (Kuang
218 et al., 2017). This simplified relationship between κ_c and κ_f is applicable for two reasons. On one
219 hand, the accurate conversion cannot be achieved without detailed information of the particle
220 hygroscopicity, which is difficult and complicated to measure. On the other hand, a deviation of κ_c
221 less than 0.1 generally leads to a deviation of N_{CCN} less than 20% (Ma et al., 2016), which is
222 comparable with the deviation of CCN measurements. As a result, for a simple method of N_{CCN}
223 calculation, this conversion is quite easy and adequate enough.

224 Besides aerosol size and hygroscopicity, aerosol mixing state can also affect aerosol cloud
225 activity. When primary aerosol emissions are strong, aerosol populations are likely to be externally
226 mixed and a realistic treatment of aerosol mixing state is critical for N_{CCN} calculation (Cubison et al.,
227 2008; Wex et al., 2010). But for regions away from strong aerosol primary emissions, the influence of
228 mixing state on aerosol cloud activity is small and the assumption of internal mixing state is effective
229 for the estimation of N_{CCN} (Dusek et al., 2006; Deng et al., 2013; Ervens et al., 2010). For regions
230 above the boundary layer where clouds form and measurements of N_{CCN} are important, this
231 conclusion is tenable if there are no plumes (Moteki and Kondo, 2007; McMeeking et al., 2011). In
232 the new method of this paper aerosol populations are assumed to be internally mixed. Thus this
233 method might not be applicable for regions or air masses greatly affected by strong primary aerosol
234 emissions. Furthermore, this new method cannot be applied for regions where sea salt or dust
235 prevails, as mentioned before. In summary, this method can be used to calculate N_{CCN} for continental
236 regions, especially at clouds forming heights, where aged aerosol particles dominate.

237 3.2. Validation based on N_{CCN} measurement

238 The method for calculating N_{CCN} based on measurement of the humidified nephelometer system,
239 including the conversion of κ_c and the lookup-table, is examined using data measured in Gucheng.

240 Overview of data in Gucheng is shown in Figure 4. From polluted periods to clean periods,
241 significant variations of N_{CCN} and σ_{sp} can be found but AR_{sp} of N_{CCN} to σ_{sp} stays around 5. On
242 October 23rd and 29th, N_{CCN} and σ_{sp} are lower than $2000\#/cm^3$ and $500Mm^{-1}$, respectively. While on



243 October 20th, 26th and November 3rd, N_{CCN} and σ_{sp} are higher than $2000\#/cm^3$ and $500Mm^{-1}$,
244 respectively. These variations of N_{CCN} and σ_{sp} are mainly due to the variation of the particle number
245 concentration rather than the particle microphysical properties. Variations of AR_{sp} result from the
246 variations of \dot{A} and κ_c , which indicate the variations of aerosol microphysical properties.

247 In general, AR_{sp} is more sensitive to variations of \dot{A} . As mentioned before, the sensitivity of
248 AR_{sp} to \dot{A} is determined by both \dot{A} and κ_f . In detail, \dot{A} during the campaign mainly ranges from
249 0.5 to 15 and κ_f ranges mainly from 0.05 to 0.2, which means that κ_c ranges from 0.25 to 0.4.
250 These values of \dot{A} and κ_f correspond a significant sensitivity of AR_{sp} to \dot{A} , as the lookup table
251 shows in figure 2. The sensitivity of AR_{sp} to κ_c is much small and only notable during some short
252 periods. For example, from November 5th to 7th, variations of κ_f and \dot{A} are opposite and result in
253 nearly constant AR_{sp} . And from October 30th to November 2nd, consistent variations of \dot{A} and κ_f
254 lead to greater variations of AR_{sp} than other periods. This weak sensitivity of AR_{sp} to κ_f may be due
255 to the uncertainty of κ_c calculated from κ_f based on the simplified conversion.

256 This simplified conversion of κ_c is examined by comparing κ_f and κ_c measured in Gucheng
257 campaign, shown in Figure 5. In general, $\Delta\kappa$ that indicates the difference between κ_f and κ_c is
258 around 0.2 and independent from \dot{A} and κ_c . Over 80% of $\Delta\kappa$ ranges from 0.1 to 0.3 that confirms
259 applicability of the simplified conversion of κ_c . However, a notable deviation of $\Delta\kappa$ can be found
260 when \dot{A} is higher than 1.5. High values of \dot{A} represent existence of small particles. Compositions
261 and mixing state of these small particles, which may be fresh emitted and experience inefficient
262 aging processes, are diverse and likely to deviate from the simplified conversion of κ_c .

263 Therefore, considering the deviation of κ_c conversion and high sensitivity of AR_{sp} to κ_c when
264 \dot{A} is higher than 1.5, the method of calculating N_{CCN} from measurements of a humidified
265 nephelometer system may lead to significant deviation in this case which means that this method can
266 only be adopted when \dot{A} is lower than 1.5.

267 Based on the lookup table of κ_c and \dot{A} , AR_{sp} is calculated and applied to calculate N_{CCN} with
268 σ_{sp} . The calculated AR_{sp} and N_{CCN} are compared with the measured AR_{sp} and N_{CCN} shown as the
269 green dots in Figure 6. In general, good agreements between calculations and measurements are



270 achieved and relative deviations are within 30%. For the comparison of AR_{sp} , the system relative
271 deviation is less than 10%. For the comparison of N_{CCN} , the slope and the correlation coefficient of
272 the regression are 1.03 and 0.966, respectively.

273 In addition, the influence of the κ_c conversion on AR_{sp} and N_{CCN} calculation are evaluated in
274 two ways. In the first way, $\Delta\kappa$ of the κ_c conversion is set to be 0.05 higher or lower, which means
275 $\Delta\kappa$ of 0.25 or 0.15. The corresponding results are presented as the red dots and blue dots in Figure 6.
276 In the second way, a constant κ_c of 0.34, which is the average of κ_c values in Gucheng campaign,
277 is used to calculate AR_{sp} and N_{CCN} , and shown as the grey dots in Figure 6. In general, differences
278 among calculations using various κ_c conversions are quite small. The $\Delta\kappa$ difference of 0.05 in κ_c
279 conversion only leads to a difference of 10% for the system relative deviation. The correlation
280 coefficient of the calculation using a constant κ_c is just a little lower than correlation coefficients of
281 calculations using a κ_c conversion. As a result, the method of calculating N_{CCN} is insensitive to the
282 uncertainty of the κ_c conversion.

283 In this study, the insensitivity of calculated N_{CCN} to κ_c conversion is partly due to the small
284 variation of κ_f during the campaign. On one hand, the variation of κ_c can be quite large and cause
285 non-ignorable deviations of calculated N_{CCN} . As previous studies of N_{CCN} measurement showed, the
286 variation of κ_c is often small and a constant κ_c can be used to calculate N_{CCN} accurately (Andreae
287 and Rosenfeld, 2008; Gunthe et al., 2009; Rose et al., 2010; Deng et al., 2013). Results in this study
288 are similar to these previous studies. However, large variations of κ_c are also found in some other
289 studies. In NCP, fluctuations of aerosol hygroscopicity during New Particle Formation events and
290 soot emissions lead to significant deviations of calculated N_{CCN} from average aerosol hygroscopicity
291 (Ma et al., 2016). On the other hand, the influence of κ_c cannot be ignored because the value of the
292 average hygroscopicity is different in various regions during various periods. In summer of NCP,
293 measured κ_f at sub-saturated conditions can reach up to 0.45 when inorganic compositions
294 dominate in particles (Kuang et al., 2016). In this case, calculated N_{CCN} ignoring κ_c may be 10 times
295 larger than measured N_{CCN} . To sum up, although the exact value of κ_c cannot be obtained from the
296 measurement of the humidified nephelometer system, the influence of κ_c on N_{CCN} can be inferred
297 and is found to be correct enough considering the convenience of this method. More data, especially
298 in observations of more hygroscopic aerosol, is still needed to confirm this method.



299 4. Conclusions

300 N_{CCN} is a key parameter of cloud microphysics and aerosol indirect radiative effect. Direct
301 measurements of N_{CCN} are generally conducted under super-saturated conditions in cloud chambers,
302 and are complex and costly. The aerosols of accumulation mode contribute most to both the aerosol
303 scattering coefficient and the aerosol CCN activity. In view of this, it is possible to predict N_{CCN}
304 based on relationships between aerosol optical properties and the aerosol CCN activity. In this study,
305 a new method is proposed to calculate N_{CCN} based on measurements of a humidified nephelometer
306 system. In this method, N_{CCN} is derived from a look-up table which involves σ_{sp} , \dot{A} and κ_f , and
307 the required three parameters can be obtained from a three-wavelength humidified nephelometer
308 system.

309 Relationships between aerosol optical properties and aerosol CCN activity are investigated using
310 datasets about aerosol PNSD measured during several campaigns in the North China Plain. The
311 relationship between σ_{sp} , \dot{A} , κ_c and N_{CCN} is analyzed. It is found that the ratio between N_{CCN} and
312 σ_{sp} , referred to as AR_{sp} , is determined by κ_c and \dot{A} . In light of this, it is possible to calculate N_{CCN}
313 based only on measurements of a three-wavelength humidified nephelometer system which provides
314 information about σ_{sp} , the hygroscopicity parameter κ and \dot{A} . However, κ derived from
315 measurements of a humidified nephelometer system under sub-saturated conditions (termed as κ_f)
316 differs from κ under super-saturated conditions which indicate CCN activity (termed as κ_c). As a
317 result, the conversion from κ_f to κ_c is needed. Based on previous studies of aerosol hygroscopicity
318 and CCN activity, a simple conversion from κ_f to κ_c with a fixed difference (referred to as $\Delta\kappa$) of
319 0.2 is proposed. On the basis of this simple conversion, the method of N_{CCN} prediction based only on
320 measurements of a humidified nephelometer system is achieved under conditions without sea salt
321 aerosol or dust aerosol.

322 This method is validated with measurements from a humidified nephelometer system and a CCN
323 counter in Gucheng in 2016. During the campaign, both N_{CCN} and σ_{sp} vary with the pollution
324 conditions. AR_{sp} is around 5 and change with \dot{A} and κ_f . The difference between κ_f and κ_c , was
325 0.2 ± 0.1 . The agreement between the calculated N_{CCN} and the measured N_{CCN} is achieved with



326 relative deviations less than 30%. Sensitivity of calculated N_{CCN} to conversions from κ_f to κ_c is
327 studied by applying different kinds of conversions. Results show that calculated N_{CCN} varies little
328 and is insensitive to the conversions, which confirms the robustness and applicability of this newly
329 proposed method.

330 This study has connected aerosol optical properties with N_{CCN} , and also proposed a novel
331 method to calculate N_{CCN} based only on measurements of a three-wavelength humidified
332 nephelometer system. Due to the simple operation and stability of the humidified nephelometer
333 system, this method will facilitate the real time monitoring of N_{CCN} , especially on aircrafts. In
334 addition, measurements of the widely used CCN counter are limited to supersaturations higher than
335 0.07. This method is more suitable for calculating N_{CCN} at lower supersaturations, thus is more
336 applicable for ambient measurements of clouds and fogs in the atmosphere.

337

338 Acknowledgement

339 This work is supported by the National Natural Science Foundation of China (41590872,
340 41375134 and 41505107).

341



342 Reference

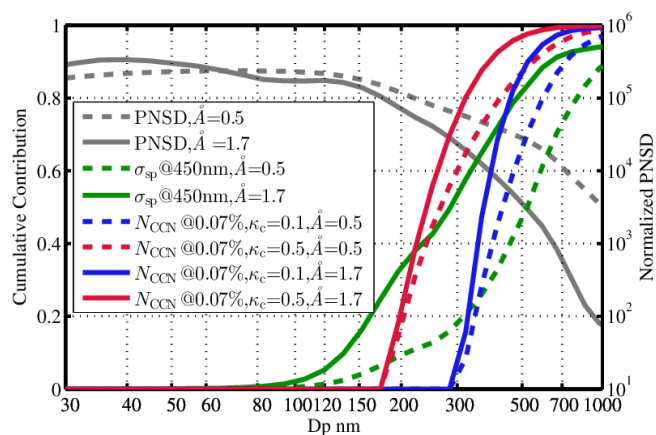
- 343 Andreae, M. O., and Rosenfeld, D.: Aerosol-cloud-precipitation interactions. Part 1. The nature and
344 sources of cloud-active aerosols, *Earth-Science Reviews*, 89, 13-41, 10.1016/j.earscirev.2008.03.001,
345 2008.
- 346 Andreae, M. O.: Correlation between cloud condensation nuclei concentration and aerosol optical
347 thickness in remote and polluted regions, *Atmospheric Chemistry and Physics*, 9, 543-556, 2009.
- 348 Brock, C. A., Wagner, N. L., Anderson, B. E., Attwood, A. R., Beyersdorf, A., Campuzano-Jost, P.,
349 Carlton, A. G., Day, D. A., Diskin, G. S., Gordon, T. D., Jimenez, J. L., Lack, D. A., Liao, J.,
350 Markovic, M. Z., Middlebrook, A. M., Ng, N. L., Perring, A. E., Richardson, M. S., Schwarz, J. P.,
351 Washenfelder, R. A., Welti, A., Xu, L., Ziemba, L. D., and Murphy, D. M.: Aerosol optical properties
352 in the southeastern United States in summer – Part 1: Hygroscopic growth, *Atmos. Chem. Phys.*, 16,
353 4987-5007, 10.5194/acp-16-4987-2016, 2016.
- 354 Chen, J., Zhao, C. S., Ma, N., and Yan, P.: Aerosol hygroscopicity parameter derived from the light
355 scattering enhancement factor measurements in the North China Plain, *Atmos. Chem. Phys.*, 14,
356 8105-8118, 10.5194/acp-14-8105-2014, 2014.
- 357 Covert, D. S., Charlson, R., and Ahlquist, N.: A study of the relationship of chemical composition
358 and humidity to light scattering by aerosols, *Journal of applied meteorology*, 11, 968-976, 1972.
- 359 Cubison, M. J., Ervens, B., Feingold, G., Docherty, K. S., Ulbrich, I. M., Shields, L., Prather, K.,
360 Hering, S., and Jimenez, J. L.: The influence of chemical composition and mixing state of Los
361 Angeles urban aerosol on CCN number and cloud properties, *Atmospheric Chemistry and Physics*, 8,
362 5649-5667, 2008.
- 363 Deng, Z. Z., Zhao, C. S., Ma, N., Liu, P. F., Ran, L., Xu, W. Y., Chen, J., Liang, Z., Liang, S., Huang,
364 M. Y., Ma, X. C., Zhang, Q., Quan, J. N., Yan, P., Henning, S., Mildenerger, K., Sommerhage, E.,
365 Schäfer, M., Stratmann, F., and Wiedensohler, A.: Size-resolved and bulk activation properties of
366 aerosols in the North China Plain, *Atmos. Chem. Phys.*, 11, 3835-3846, 10.5194/acp-11-3835-2011,
367 2011.
- 368 Deng, Z. Z., Zhao, C. S., Ma, N., Ran, L., Zhou, G. Q., Lu, D. R., and Zhou, X. J.: An examination
369 of parameterizations for the CCN number concentration based on in situ measurements of aerosol
370 activation properties in the North China Plain, *Atmos. Chem. Phys.*, 13, 6227-6237,
371 10.5194/acp-13-6227-2013, 2013.
- 372 Dusek, U., Frank, G., Hildebrandt, L., Curtius, J., Schneider, J., Walter, S., Chand, D., Drewnick, F.,
373 Hings, S., and Jung, D.: Size matters more than chemistry for cloud-nucleating ability of aerosol
374 particles, *Science*, 312, 1375-1378, 2006.
- 375 Ervens, B., Cubison, M., Andrews, E., Feingold, G., Ogren, J. A., Jimenez, J. L., DeCarlo, P., and
376 Nenes, A.: Prediction of cloud condensation nucleus concentration using measurements of
377 aerosol size distributions and composition and light scattering enhancement due to humidity, *Journal*
378 *of Geophysical Research: Atmospheres*, 112, n/a-n/a, 10.1029/2006jd007426, 2007.
- 379 Ervens, B., Cubison, M. J., Andrews, E., Feingold, G., Ogren, J. A., Jimenez, J. L., Quinn, P. K.,
380 Bates, T. S., Wang, J., Zhang, Q., Coe, H., Flynn, M., and Allan, J. D.: CCN predictions using
381 simplified assumptions of organic aerosol composition and mixing state: a synthesis from six
382 different locations, *Atmospheric Chemistry and Physics*, 10, 4795-4807, 10.5194/acp-10-4795-2010,
383 2010.
- 384 Gasso, S., and Hegg, D. A.: On the retrieval of columnar aerosol mass and CCN concentration by
385 MODIS, *J. Geophys. Res.-Atmos.*, 108, 401010.1029/2002jd002382, 2003.



- 386 Ghan, S. J., and Collins, D. R.: Use of in situ data to test a Raman lidar-based cloud condensation
387 nuclei remote sensing method, *Journal of Atmospheric and Oceanic Technology*, 21, 387-394,
388 10.1175/1520-0426(2004)021<0387:uoidt>2.0.co;2, 2004.
- 389 Ghan, S. J., Rissman, T. A., Elleman, R., Ferrare, R. A., Turner, D., Flynn, C., Wang, J., Ogren, J.,
390 Hudson, J., Jonsson, H. H., VanReken, T., Flagan, R. C., and Seinfeld, J. H.: Use of in situ cloud
391 condensation nuclei, extinction, and aerosol size distribution measurements to test a method for
392 retrieving cloud condensation nuclei profiles from surface measurements, *J. Geophys. Res.-Atmos.*,
393 111, D05s1010.1029/2004jd005752, 2006.
- 394 Gunthe, S. S., King, S. M., Rose, D., Chen, Q., Roldin, P., Farmer, D. K., Jimenez, J. L., Artaxo, P.,
395 Andreae, M. O., Martin, S. T., and Poschl, U.: Cloud condensation nuclei in pristine tropical
396 rainforest air of Amazonia: size-resolved measurements and modeling of atmospheric aerosol
397 composition and CCN activity, *Atmospheric Chemistry and Physics*, 9, 7551-7575, 2009.
- 398 Hudson, J. G.: AN INSTANTANEOUS CCN SPECTROMETER, *Journal of Atmospheric and*
399 *Oceanic Technology*, 6, 1055-1065, 10.1175/1520-0426(1989)006<1055:aics>2.0.co;2, 1989.
- 400 Jefferson, A.: Empirical estimates of CCN from aerosol optical properties at four remote sites, *Atmos.*
401 *Chem. Phys.*, 10, 6855-6861, 10.5194/acp-10-6855-2010, 2010.
- 402 Köhler, H.: The nucleus in and the growth of hygroscopic droplets, *Transactions of the Faraday*
403 *Society*, 32, 1152-1161, 1936.
- 404 Kapustin, V. N., Clarke, A. D., Shinzuka, Y., Howell, S., Brekhovskikh, V., Nakajima, T., and
405 Higurashi, A.: On the determination of a cloud condensation nuclei from satellite: Challenges and
406 possibilities, *J. Geophys. Res.-Atmos.*, 111, D0420210.1029/2004jd005527, 2006.
- 407 Kreidenweis, S. M., and Asa-Awuku, A.: 5.13 - Aerosol Hygroscopicity: Particle Water Content and
408 Its Role in Atmospheric Processes A2 - Holland, Heinrich D, in: *Treatise on Geochemistry (Second*
409 *Edition)*, edited by: Turekian, K. K., Elsevier, Oxford, 331-361, 2014.
- 410 Kuang, Y., Zhao, C. S., Ma, N., Liu, H. J., Bian, Y. X., Tao, J. C., and Hu, M.: Deliquescent
411 phenomena of ambient aerosols on the North China Plain, *Geophys. Res. Lett.*, n/a-n/a,
412 10.1002/2016gl070273, 2016.
- 413 Kuang, Y., Zhao, C., Tao, J., Bian, Y., Ma, N., and Zhao, G.: A novel method to derive the aerosol
414 hygroscopicity parameter based only on measurements from a humidified nephelometer system,
415 *Atmos. Chem. Phys. Discuss.*, 2017, 1-25, 10.5194/acp-2016-1066, 2017.
- 416 Lance, S., Nenes, A., Medina, J., and Smith, J.: Mapping the operation of the DMT continuous flow
417 CCN counter, *Aerosol science and technology*, 40, 242-254, 2006.
- 418 Latham, T. L., and Nenes, A.: Water Vapor Depletion in the DMT Continuous-Flow CCN Chamber:
419 Effects on Supersaturation and Droplet Growth, *Aerosol science and technology*, 45, 604-615,
420 10.1080/02786826.2010.551146, 2011.
- 421 Liu, J. J., and Li, Z. Q.: Estimation of cloud condensation nuclei concentration from aerosol optical
422 quantities: influential factors and uncertainties, *Atmospheric Chemistry and Physics*, 14, 471-483,
423 10.5194/acp-14-471-2014, 2014.
- 424 Ma, N., Zhao, C., Nowak, A., Müller, T., Pfeifer, S., Cheng, Y., Deng, Z., Liu, P., Xu, W., and Ran, L.:
425 Aerosol optical properties in the North China Plain during HaChi campaign: an in-situ optical
426 closure study, *Atmos. Chem. Phys.*, 11, 5959-5973, 2011.
- 427 Ma, N., Zhao, C., Tao, J., Wu, Z., Kecorius, S., Wang, Z., Groß, J., Liu, H., Bian, Y., Kuang, Y., Teich,
428 M., Spindler, G., Müller, K., van Pinxteren, D., Herrmann, H., Hu, M., and Wiedensohler, A.:
429 Variation of CCN activity during new particle formation events in the North China Plain, *Atmos.*



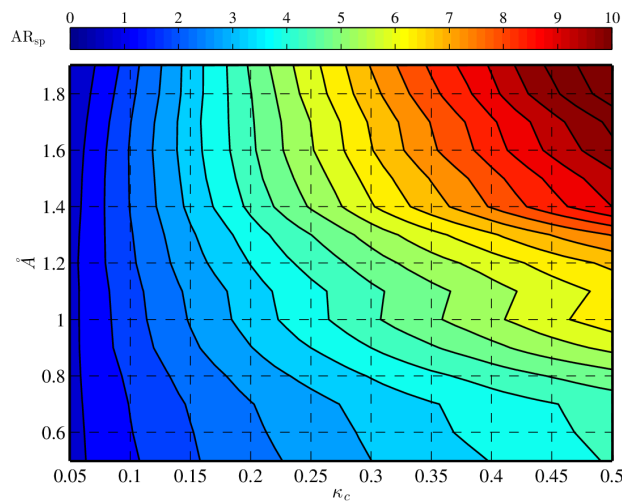
- 430 Chem. Phys., 16, 8593-8607, 10.5194/acp-16-8593-2016, 2016.
- 431 McMeeking, G. R., Morgan, W. T., Flynn, M., Highwood, E. J., Turnbull, K., Haywood, J., and Coe,
432 H.: Black carbon aerosol mixing state, organic aerosols and aerosol optical properties over the
433 United Kingdom, Atmos. Chem. Phys., 11, 9037-9052, 10.5194/acp-11-9037-2011, 2011.
- 434 Moteki, N., and Kondo, Y.: Effects of Mixing State on Black Carbon Measurements by
435 Laser-Induced Incandescence, Aerosol science and technology, 41, 398-417,
436 10.1080/02786820701199728, 2007.
- 437 Nenes, A., Chuang, P. Y., Flagan, R. C., and Seinfeld, J. H.: A theoretical analysis of cloud
438 condensation nucleus (CCN) instruments, J. Geophys. Res.-Atmos., 106, 3449-3474,
439 10.1029/2000jd900614, 2001.
- 440 Petters, M. D., and Kreidenweis, S. M.: A single parameter representation of hygroscopic growth and
441 cloud condensation nucleus activity, Atmospheric Chemistry and Physics, 7, 1961-1971, 2007.
- 442 Roberts, G., and Nenes, A.: A continuous-flow streamwise thermal-gradient CCN chamber for
443 atmospheric measurements, Aerosol science and technology, 39, 206-221, 2005.
- 444 Rose, D., Gunthe, S., Mikhailov, E., Frank, G., Dusek, U., Andreae, M., and Pöschl, U.: Calibration
445 and measurement uncertainties of a continuous-flow cloud condensation nuclei counter
446 (DMT-CCNC): CCN activation of ammonium sulfate and sodium chloride aerosol particles in theory
447 and experiment, Atmospheric Chemistry and Physics, 8, 1153-1179, 2008.
- 448 Rose, D., Nowak, A., Achtert, P., Wiedensohler, A., Hu, M., Shao, M., Zhang, Y., Andreae, M. O.,
449 and Pöschl, U.: Cloud condensation nuclei in polluted air and biomass burning smoke near the
450 mega-city Guangzhou, China - Part 1: Size-resolved measurements and implications for the
451 modeling of aerosol particle hygroscopicity and CCN activity, Atmospheric Chemistry and Physics,
452 10, 3365-3383, 2010.
- 453 Shinzuka, Y., Clarke, A. D., Nenes, A., Jefferson, A., Wood, R., McNaughton, C. S., Ström, J.,
454 Tunved, P., Redemann, J., Thornhill, K. L., Moore, R. H., Latham, T. L., Lin, J. J., and Yoon, Y. J.:
455 The relationship between cloud condensation nuclei (CCN) concentration and light extinction of
456 dried particles: indications of underlying aerosol processes and implications for satellite-based CCN
457 estimates, Atmos. Chem. Phys., 15, 7585-7604, 10.5194/acp-15-7585-2015, 2015.
- 458 Titos, G., Cazorla, A., Zieger, P., Andrews, E., Lyamani, H., Granados-Muñoz, M. J., Olmo, F. J., and
459 Alados-Arboledas, L.: Effect of hygroscopic growth on the aerosol light-scattering coefficient: A
460 review of measurements, techniques and error sources, Atmos. Environ., 141, 494-507,
461 <http://dx.doi.org/10.1016/j.atmosenv.2016.07.021>, 2016.
- 462 Wex, H., McFiggans, G., Henning, S., and Stratmann, F.: Influence of the external mixing state of
463 atmospheric aerosol on derived CCN number concentrations, Geophys. Res. Lett., 37, L10805
464 10.1029/2010gl043337, 2010.
- 465 Whitehead, J. D., Irwin, M., Allan, J. D., Good, N., and McFiggans, G.: A meta-analysis of particle
466 water uptake reconciliation studies, Atmos. Chem. Phys., 14, 11833-11841,
467 10.5194/acp-14-11833-2014, 2014.
- 468 Wu, Z. J., Poulain, L., Henning, S., Dieckmann, K., Birmili, W., Merkel, M., van Pinxteren, D.,
469 Spindler, G., Mueller, K., Stratmann, F., Herrmann, H., and Wiedensohler, A.: Relating particle
470 hygroscopicity and CCN activity to chemical composition during the HCCT-2010 field campaign,
471 Atmospheric Chemistry and Physics, 13, 7983-7996, 10.5194/acp-13-7983-2013, 2013.



474

475 Figure 1.

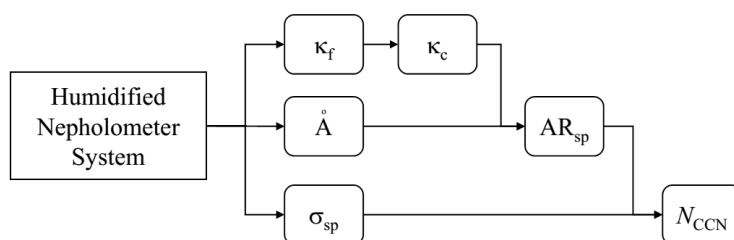
476 Aerosol PNSD (black lines), the cumulative contribution of σ_{sp} at wavelength of 450nm (green
 477 lines) and N_{CCN} at supersaturation of 0.07% (red and blue lines) based on measurement in several
 478 campaigns in the North China Plain. Solid lines and dashed lines indicate \AA of 1.7 and 0.5,
 479 respectively. Blue lines and red lines indicate κ_c of 0.1 and 0.5, respectively.



480

481 Figure 2.

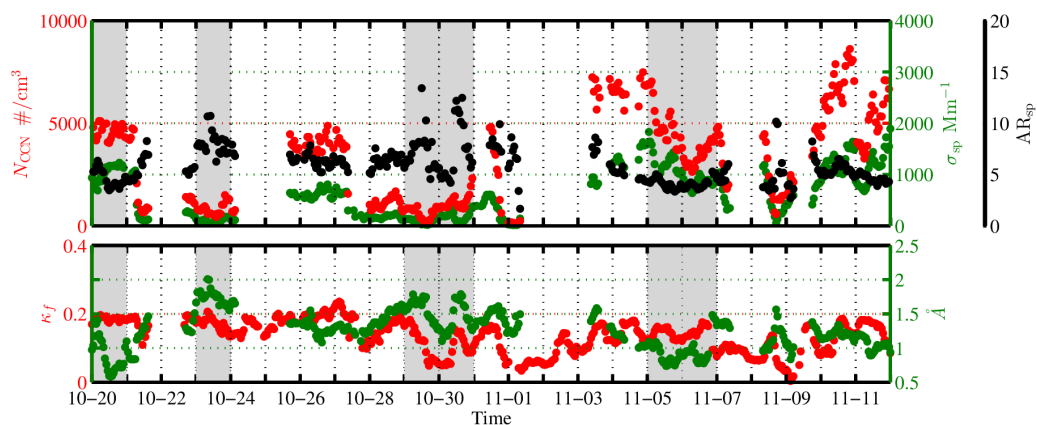
482 Colors represent AR_{sp} (ratios between N_{CCN} and σ_{sp}) with κ_c and \AA .



483

484 Figure 3.

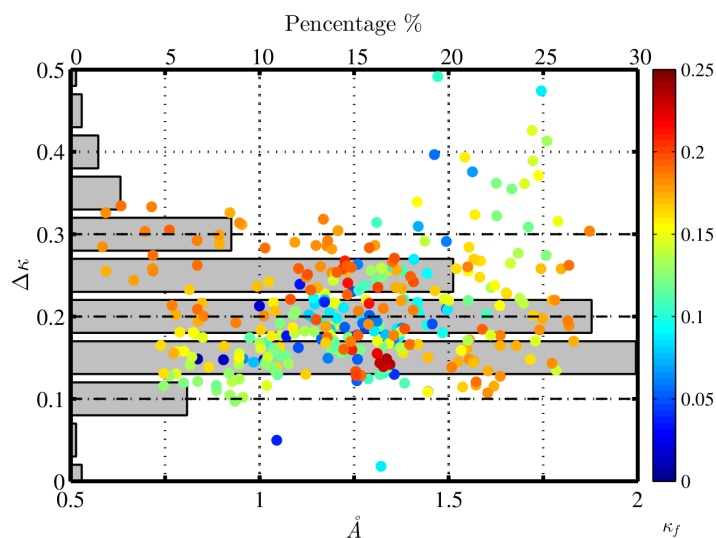
485 The schematic chart of the N_{CCN} prediction based on measurements of a humidified nephelometer
 486 system.



487

488 Figure 4.

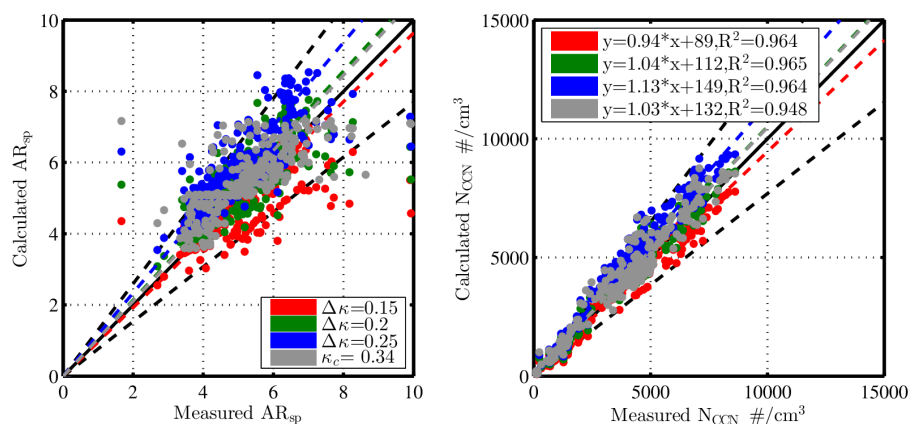
489 Overview of measurements in Gucheng in 2016. Upper plot: time series of N_{CCN} at the
 490 supersaturation of 0.07% (red dots), σ_{sp} at the wavelength of 50nm (green dots) and their ratios
 491 (black dots), referred to as AR_{sp} . Lower plot: time series of κ_f (red dots) and \dot{A} (green dots).



492

493 Figure 5.

494 Differences between κ_c and κ_f , referred to as $\Delta\kappa$, with \AA (positions of dots) and κ_f (colors of
 495 dots). Bars represent percentages of $\Delta\kappa$ within different ranges.



496

497 Figure 6.

498 Left plot: comparisons of calculated AR_{sp} and measured AR_{sp} with different conversions of κ_c from
 499 κ_f . Right plot: regressions of calculated N_{CCN} and measured N_{CCN} with different conversions of κ_c
 500 from κ_f .